EUMETSAT

OSI SAF

OCEAN AND SEA ICE

Algorithm Theoretical Basis Document for the scatterometer wind products

All scatterometer wind products in the ranges OSI-100 to OSI-115 and OSI-150 to OSI-159

Version: 2.1

Date: 12/10/2022

Ocean and Sea Ice SAF

Royal Netherlands
Meteorological Institute
*Ministry of Infrastructure
and Water Management*

Document Change record

Document version	Software version	Date	Author	Change description
1.0		Aug 2012	AV	Initial version
1.1		Feb 2014	AV	Changes resulting from SeaWinds reprocessing RR and PCR
1.2		Feb 2015	AV	Editorial changes for RapidScat
1.3		Jun 2016	AV	Editorial changes for OSCAT reprocessing RR and PCR, included review comments
1.4		Feb 2017	AV	Changes resulting from ERS reprocessing DRR
1.5		Feb 2017	AV	Comments from ScatSat PCR included
1.6		May 2018	AV	Implementation of CMOD7 for ASCAT and stress-equivalent model winds
1.7		Oct 2018	AV	Version for Requirement Review and Product Consolidation Review of wind data records
1.8		Oct 2019	AV, AS	Version for Requirement Review and Product Consolidation Review of HY-2B and CFOSAT
1.9		Feb 2020	AV	Version for EPS-SG PDCR: information on SCA winds added
2.0		May 2021	AV	Version for Operational Readiness Review of HY-2B and HY-2C
2.1		Oct 2022	AV	Version for Delivery Readiness Review of Ku-band data records

Table of contents

1. Introduction

The EUMETSAT Ocean and Sea Ice Satellite Application Facility (OSI SAF) produces a range of air-sea interface products, namely: wind, sea ice characteristics, Sea Surface Temperatures (SST) and radiative fluxes, Surface Solar Irradiance (SSI) and Downward Long wave Irradiance (DLI).

KNMI is involved in the OSI SAF as the centre where the level 1 to level 2 scatterometer wind processing is carried out. This document is the Algorithm Theoretical Basis Document to the wind products. More general information on the OSI SAF project is available on the OSI SAF web site: https://osi-saf.eumetsat.int/. Information about the specific wind products and their status can be found on https://scatterometer.knmi.nl/.

The scatterometer is an instrument that provides information on the wind field near the ocean surface, and scatterometry is the knowledge of extracting this information from the instrument's output [1]. Space-based scatterometry has become of great benefit to meteorology [2][3], oceanography [4] and climate [5] in the past years.

KNMI has a long experience in scatterometer processing and is developing generic software for this purpose. Processing systems have been developed for the ERS, NSCAT, SeaWinds, ASCAT, Oceansat-2/OSCAT, RapidScat, Haiyang 2/HSCAT, ScatSat1/OSCAT, and CFOSAT scatterometers. Scatterometer processing software is developed in the OSI SAF and provided through the EUMETSAT Numerical Weather Prediction Satellite Application Facility (NWP SAF), and is used in the wind processing performed operationally in the OSI SAF. The algorithms developed for the various steps in the wind retrieval are shared between the processing software for the different instruments, but some details differ depending on instrument characteristics like antenna configuration and frequency band used. This document provides a general overview and also briefly describes the differences between the instruments. The wind processing software package for C-band scatterometers (ASCAT Wind Data Processor, AWDP for ERS and ASCAT) is described in [6], the software package for Ku-band pencil beam scatterometers (Pencil Beam Wind Processor, PenWP for SeaWinds, RapidScat, OSCAT and HSCAT) is described in [7], and the software package for Ku-band rotating fan beam scatterometers (CFOSAT Wind Data Processor, CWDP) is described in [8].

Web resources that may be consulted and which complement this ATBD are:

- KNMI scatterometer website;

- SCA science plan;

- KNMI publications website;

- Training courses on applications of satellite wind and wave products for marine forecasting, available in video (Oostende 2011) or document forms (Lisbon 2018);

- International Ocean Vector Winds Science Team meeting presentations;

Following the introduction, section 2 of this document presents an overview of the various scatterometer instrument concepts, section 3 provides the processing algorithms and section 4 gives a brief overview of the wind processing of the different products in near-real time. Please note that this document is limited to a qualitative description of the algorithms, including strengths and weaknesses, but without presenting too many formulas. This is done to increase the readability. The algorithms are more detailed in the references provided.

2. Scatterometer instrument concepts

The scatterometer is a non-nadir looking real aperture radar instrument. Wind vector information over the oceans can be empirically derived from it. Over the last decades, scatterometers on-board satellites have provided very valuable sea surface wind field information. In addition to the meteorological and oceanographic use of scatterometer winds, the scatterometer data are of interest in applications such as sea ice detection [9] and land surface soil moisture and rain determination [10]. In terms of antenna geometry, the scatterometer systems can be classified as side-looking and rotating scatterometers. Space-borne scatterometer instruments are always mounted on low Earth orbiting platforms, most of the time polar orbiters. As a consequence of this, a specific location on Earth will normally be re-visited twice a day at maximum.

Side-looking scatterometers consist of a set of static fan-beam antennas pointing to one or both sides of the satellite flight track. Examples of such instruments are the NASA Scatterometer (NSCAT) on-board ADEOS-1, the scatterometers on the European Remote Sensing Satellites ERS-1 and ERS-2 [12], the Advanced SCATterometer (ASCAT) on-board Metop and its future successor SCA on-board of the European Polar System - Second Generation (EPS-SG) [1]. Examples of the illumination pattern of side-looking scatterometers are shown in Figure 1. These patterns show the coverages of ASCAT and SCA which have, contrary to ERS, two sets of antennas looking to either side of the satellite ground track. ERS only has one set of three antennas looking to the right side of the satellite track. These scatterometers have a rather constant observation quality across the swath.
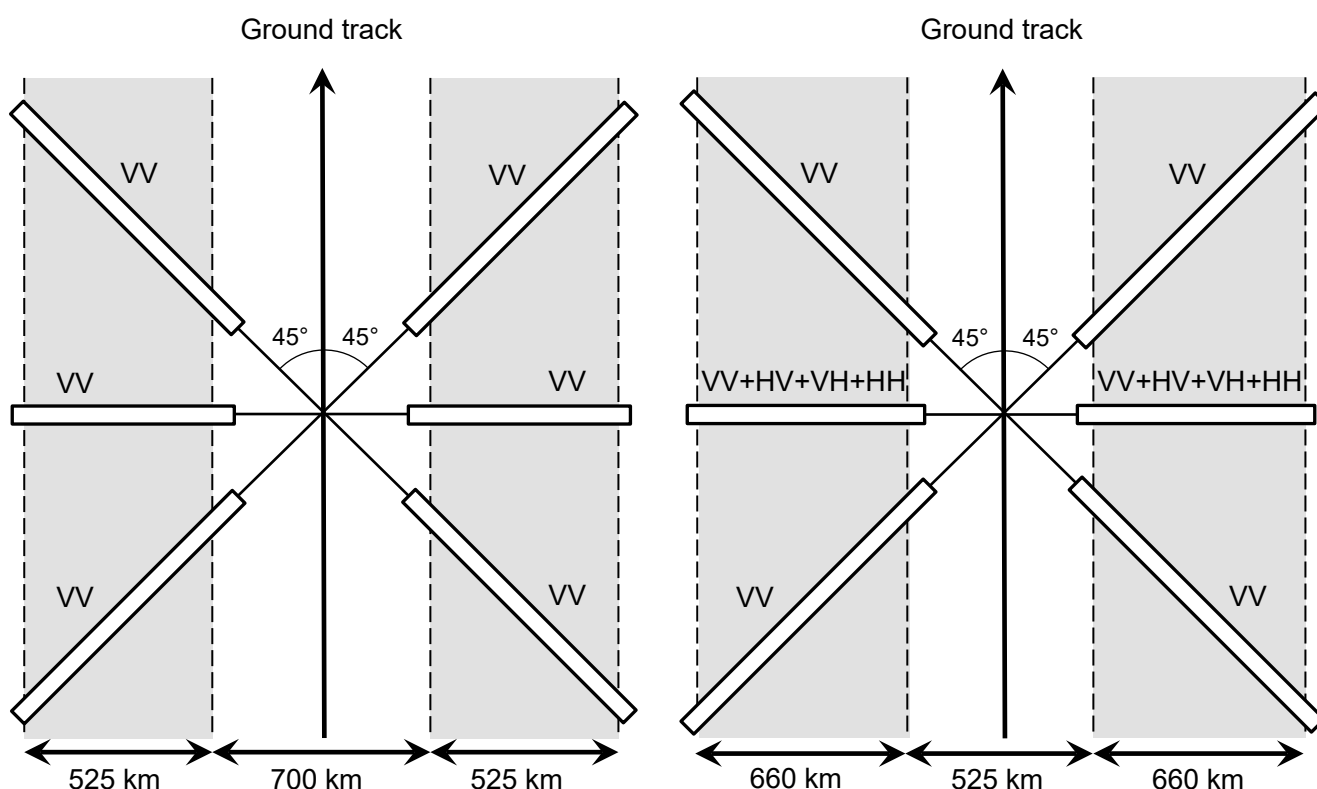

Figure 1: Earth surface coverage of the scans of the side-looking ASCAT scatterometer (left) and the SCA scatterometer (right). Each location in the swaths is illuminated by the fore, the mid, and the aft beam as the satellite propagates towards the top of the page.

SCA on EPS-SG has the same geometry as ASCAT, but the incidence angle range is larger, resulting in somewhat broader left and right swaths, as is shown in the right hand side of Figure 1. Moreover, the spatial resolution of SCA is better and it has cross-polarisation (HV and VH) and horizontal polarisation (HH) measurements on the mid beams. The HV and VH measurements increase the sensitivity and accuracy at high wind speeds.

In contrast to side-looking scatterometers, the rotating scatterometers have a set of rotating antennas that sweep the Earth surface in a circular pattern as the satellite moves. The earlier antennas were pencil (or spot) beams, as used for SeaWinds on-board QuikSCAT, OSCAT on-board Oceansat-2, RapidScat on-board the International Space Station, and HSCAT on-board of HY-2A, HY-2B, HY-2C, and HY-2D. See Figure 2 for the ground illumination pattern of SeaWinds, OSCAT, or HSCAT. Due to the conical scanning, a swath location is generally viewed by each pencil beam when looking forward (fore) and a second time when looking aft. As such, up to four measurement classes (called "view" here) emerge: horizontally polarised (HH) fore, HH aft, vertically polarised (VV) fore, and VV aft, in each Wind Vector Cell (WVC).
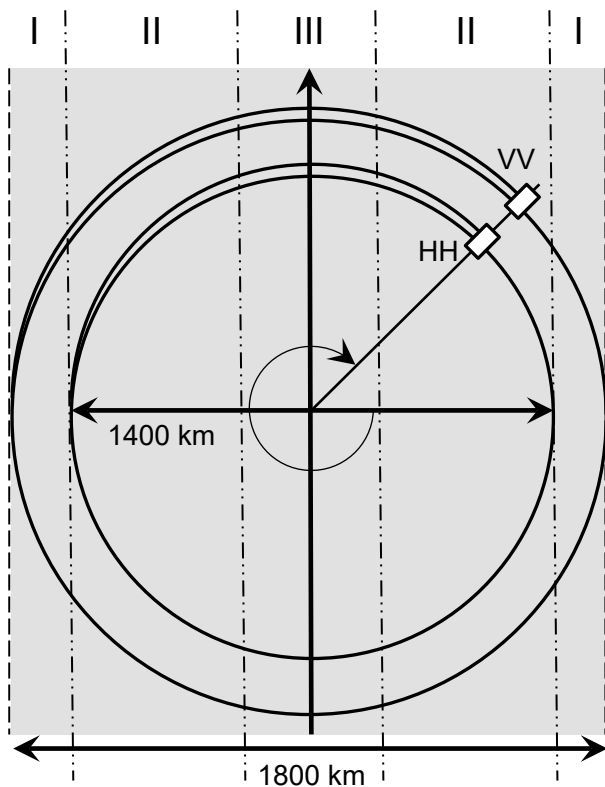

Figure 2: Earth surface coverage of the scans of the HH and VV pencil-beams of SeaWinds, OSCAT, and HSCAT. As the satellite propagates towards the top of the page the swath (in grey) is illuminated, and three areas are discriminated:
I: Outer swath: only viewed once by the VV beam in the forward direction, and once in the aft direction (2 views), the azimuth view directions are very close and perpendicular to the satellite propagation direction;
II: Sweet (inner) swath: Viewed both by the VV and HH beam, both in fore and aft direction (4 views), the azimuth views are very diverse in direction;
III: Nadir (inner) swath: As II, but the azimuth view direction is close to the satellite propagation direction, or just opposite to it.

The 1800-km-wide swath covers 90% of the ocean surface in 24 hours which represents a substantial improvement compared to the side-looking scatterometers like ERS and ASCAT, but at the expense of more noise and associated wind direction ambiguity.

Recently, rotating fan beams are also being used for the scatterometer on board CFOSAT. Figure 3 shows the ground illumination pattern for CFOSAT. The fan beam uses alternating HH and VV polarisation and the incidence angle ranges between 28° and 51°. The antenna rotation speed is lower than the rotation speed of pencil beam scatterometers, ~3.5 rotations per minute vs. ~18 rotations per minute. In such a configuration, each WVC is scanned multiple times with different incidence angles in both the forward looking and aft looking directions. The average number of views (a view being a fixed combination of polarisation, incidence angle, and antenna azimuth angle) in a WVC ranges between 8 and 15, depending on the location across the swath [65]. In fact, the rotation speed of CFOSAT is so slow that the satellite propagates more than the distance between WVC rows during one antenna rotation. This means that the nadir WVCs contain different views (in terms of incidence angles) for subsequent rows. This may lead to different systematic wind errors from row to row in WVCs, mainly in nadir. The impact of this on the wind field is subject to further study.
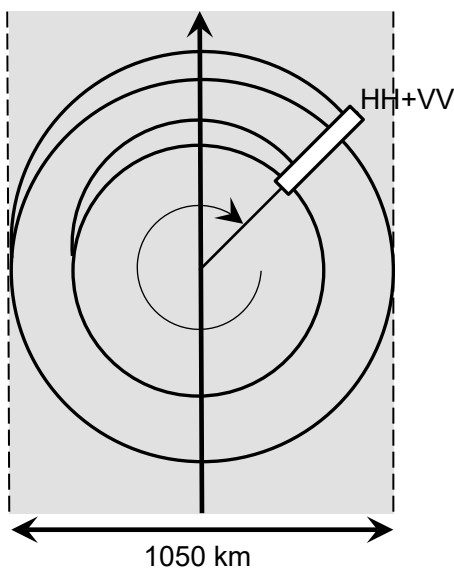

Figure 3: Earth surface coverage of the scans of the HH and VV fan-beams of CFOSAT. As the satellite propagates towards the top of the page the swath (in grey) is illuminated.

The wind retrieval from measurements of rotating scatterometers is more complex. In contrast with the side-looking scatterometers, the number of measurements and the beam azimuth angles vary with the sub-satellite cross-track location (see Figure 2 and Figure 3). In the outer swath of pencil-beam instruments the retrieval is most difficult, since here only VV-polarised data are available. The wind retrieval skill will therefore depend on the position in the swath, wind speed and wind direction. A detailed discussion of this matter is provided in [11]; pages 22-23. A detailed performance comparison study of different scatterometer concepts, based on simulation, is provided in [64] and [65].

Enhanced resolution scatterometer wind and ice products have been developed on the 5-km scale. A limitation in the spatial resolution of scatterometers is due to the size of each view, which has typical dimensions in length and width in the range of 2 to 20 km. Besides small view dimensions, high-

resolution wind vector retrieval also requires that the different views used, illuminate the same ocean area, i.e., have overlapping Spatial Response Functions (SRF) [14]. This is most complex to arrange for rotating scatterometer concepts. On the other hand, over isotropic sea ice and land surfaces, deconvolution techniques may be employed for resolution enhancement using partly overlapping views [15].

Apart from the antenna configuration, scatterometers can also be distinguished with respect to the radar frequency band. The commonly used bands are C-band (~5.25 GHz or ~5 cm wavelength) and Ku-band (~13.5 GHz or ~2 cm wavelength). The smaller wavelength of Ku-band allows either a better spatial resolution for a given antenna size or a smaller antenna size for a given spatial resolution. On the other hand, the atmosphere is not transparent at Ku-band wavelengths and in particular rain is detrimental for wind computation. In fact, moderate and heavy rain cause bogus wind retrievals of 15-20 m/s wind speed [60] and rain contamination needs to be eliminated by a quality control step [13].

Land and sea ice contamination of a WVC will seriously disturb the wind retrieval. Land can be filtered out using a fixed land-sea mask. Discrimination of water and sea ice surfaces is generally best possible when both VV and HH polarisation measurements are available like for pencil beam scatterometers [16]. For ERS and ASCAT, which only have VV-polarised measurements available, the ice screening is more difficult, but still well possible [17]. An ice discrimination algorithm for the rotating fan beam scatterometer (CFOSAT) is still in development based on [16]. In addition, prior wind and Sea Surface Temperature information can be used to prevent erratic winds over sea ice surfaces.

3. Algorithms

Scatterometry was developed heuristically. It was found experimentally that the sensitivity to wind speed and direction well describes the changes in backscatter over the ocean at moderate incidence angles due to changes in surface roughness. This is depicted in Figure 4 [18]. In return, backscatter measurements can be used to determine the wind speed and wind direction in a WVC. In addition physically-based models are developed using space-based scatterometer measurements and are useful to physically relate backscatter measurements at different wavelength and polarizations [19], though these lack the accuracy of the empirically-derived Geophysical Model Functions (GMF).

A schematic illustration of the processing is given in Figure 5. After defining the wind output and motivating the GMF that is used, the algorithms developed at KNMI are described.
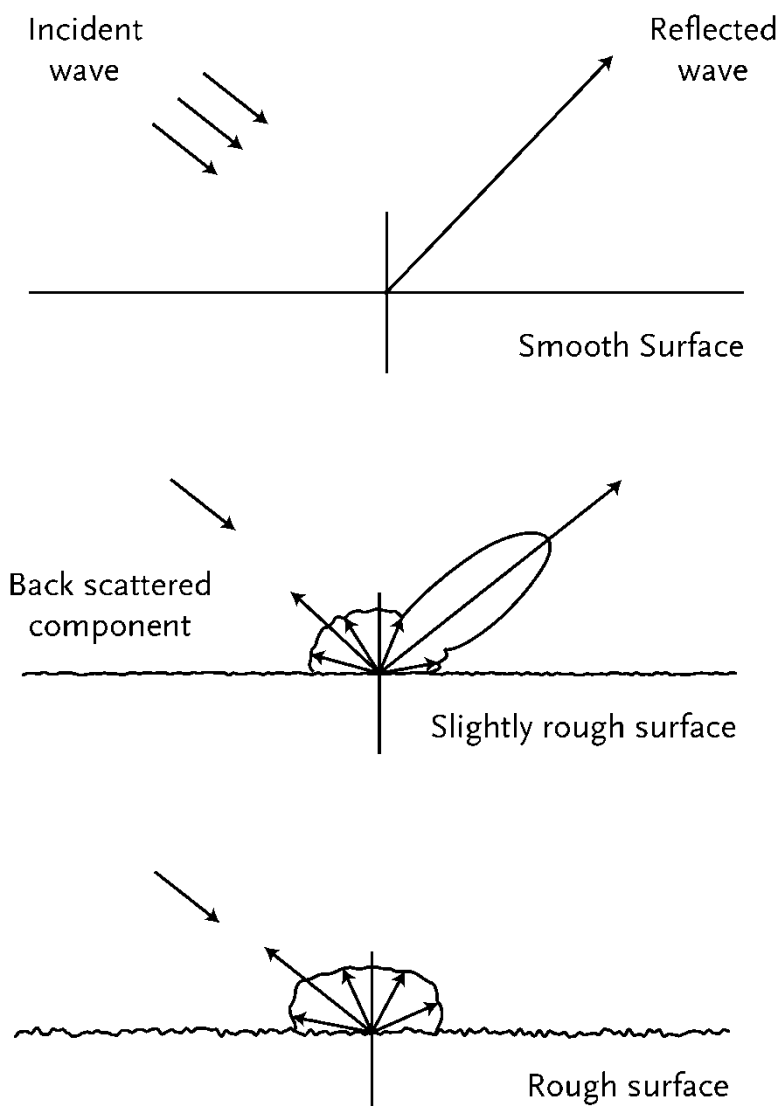

Figure 4: Schematic representation of microwave scattering and reflection at a smooth (top), rough (middle) and very rough (bottom) ocean surface. As the roughness increases more microwave power is returned towards the direction of the microwave source.

Figure 6 shows a schematic overview of the input data, ancillary data, and output data relevant to the scatterometer wind processing. For all instruments, the Level 1 input products contain the elements contained in 'General information' and 'Beam information', although the data formats are different. The 'Ancillary information' is obtained from NWP model data. The output files produced by the wind processing (in BUFR format or NetCDF format), always contain the 'General information', 'Ancillary information', and 'Wind information'. On top of that, the BUFR format data also contain the 'Beam information'.
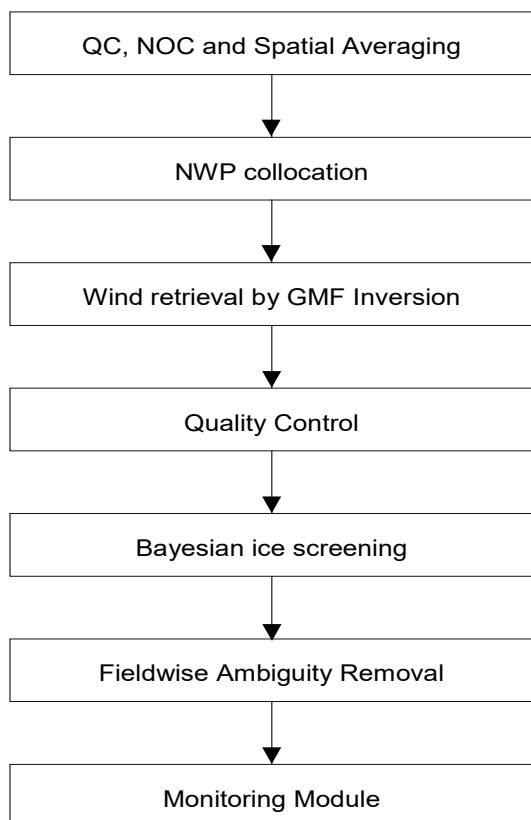
```
┌─────────────────────────────────────┐
│   QC, NOC and Spatial Averaging      │
└─────────────────────────────────────┘
                  │
                  ▼
┌─────────────────────────────────────┐
│           NWP collocation            │
└─────────────────────────────────────┘
                  │
                  ▼
┌─────────────────────────────────────┐
│     Wind retrieval by GMF Inversion  │
└─────────────────────────────────────┘
                  │
                  ▼
┌─────────────────────────────────────┐
│           Quality Control            │
└─────────────────────────────────────┘
                  │
                  ▼
┌─────────────────────────────────────┐
│        Bayesian ice screening        │
└─────────────────────────────────────┘
                  │
                  ▼
┌─────────────────────────────────────┐
│     Fieldwise Ambiguity Removal      │
└─────────────────────────────────────┘
                  │
                  ▼
┌─────────────────────────────────────┐
│          Monitoring Module           │
└─────────────────────────────────────┘
```

Figure 5: Overview of wind retrieval algorithm, QC denotes Quality Control and NOC denotes NWP Ocean Calibration.

General information (input)
- Satellite identifier
- Instrument identifier
- Orbit number
- Date and time
- Latitude and Longitude

Ancillary information (input)
- NWP model wind speed and direction

Beam information (input)
- Latitude and Longitude
- Azimuth angle
- Incidence angle
- Polarisation
- Normalised Radar Cross Section (sigma0)
- Noise value (Kp)
- Quality information

Wind information (output), multiple solutions are given with an index to the selected one
- Wind speed and direction of solution
- Backscatter distance (MLE) of solution
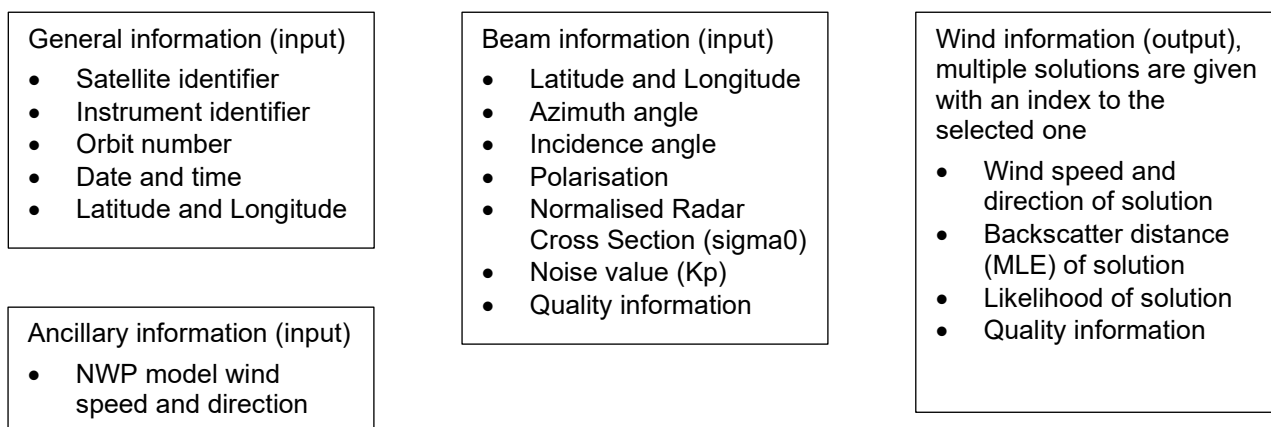- Likelihood of solution
- Quality information

Figure 6: Overview of input data, ancillary data and output data used in wind processing.

3.1. Wind definition

A scatterometer measurement relates to the ocean surface roughness (see Figure 4), while the scatterometer product is represented by the stress-equivalent wind at 10 meter height (U10S) over a WVC. The stress-equivalent wind transforms the sea surface roughness measurements to 10 m height in a unique way and independent of atmospheric properties such as its mass density and stratification [37]. Moreover, SE winds are straightforward to compute at most buoy locations and from NWP model output for validation and comparison.

For NWP model winds, the conversion from real 10m winds to SE winds goes in two steps: firstly equivalent neutral (EN) winds are computed from real winds, sea surface temperature, air temperature, Charnock parameter and specific humidity, using a stand-alone implementation of the ECMWF model surface layer physics [38]. Note that this step may be not needed if the equivalent neutral winds are available directly from model output as for example in the ECMWF operational model (since 2007) or ERA5 re-analysis. The equivalent neutral winds subsequently are converted to stress-equivalent winds (U10S) by multiplying by a correction factor of $\sqrt{(\rho/\langle\rho\rangle)}$, where ρ is the air mass density and $\langle\rho\rangle$ is the average air mass density (1.225 kg/m^3) [40].

The correction factor follows from the fact that the surface roughness as measured by the scatterometer is more closely correlated with surface stress τ than with the actual wind speed at 10 m. The surface stress τ is proportional to the air mass density and to the square of the equivalent neutral 10 m wind. In order to make the NWP winds equivalent to the scatterometer winds, we need to apply a correction, i.e., multiply by the square root of the normalised density. The air mass density is computed from the NWP model mean sea level pressure (msl), specific humidity (q) and air temperature (T) as $\rho = msl / (287.04 \times (1 + 0.6078 \times q) \times T)$ [39].

Note that in the conversion of real winds to U10S, wind turning is assumed negligible in the lowest 10 metres, the so-called surface layer, so the direction of both winds will be the same. Typically, the largest difference is related to stability effects. Since the atmospheric boundary layer is on average weakly unstable, U10S will be on average slightly stronger than the real wind by approximately 0.1 to 0.2 m/s. Besides variations due to the local weather, there are typical seasonal variations. Generally, the U10S speeds are more positively biased in colder regions and more negatively biased in warmer regions. More statistics are shown in [40].

It is important to realize that in the approach followed here the radar backscatter measurement σ^0 is related to the wind at 10 meter height above the ocean surface, simply because such wind measurements are widely available for validation as 10 m is a World Meteorological Organization (WMO) reference height. This means that any effect that relates to the mean wind vector at 10 meter height is incorporated in the backscatter-to-wind relationship. As such, the appearance of surface slicks, and the amplitude of gravity or longer ocean waves, depend to some degree on the strength of the wind and may, to the same degree, be fitted by a Geophysical Model Function, GMF ([20], Chapter I). Stoffelen ([20], Chapter IV) discusses a unique method to determine the accuracy of scatterometer, buoy, and NWP model winds by triple collocation.

At low wind speeds the wind direction and speed may vary considerably within the WVC. Locally, below a speed of roughly 2 m/s calm areas are present where little or no backscatter occurs, perhaps further extended in the presence of natural slicks that increase the water surface tension [21]. However, given the variability of the wind within a footprint area of 25 km it is, even in the case of zero mean vector wind, very unlikely that there are no patches with roughness in the footprint. As the mean vector wind

increases, the probability of a calm patch will quickly decrease, and the mean microwave backscatter will increase. Also, natural slicks quickly disappear as the wind speed increases, and as such the occurrence of these is correlated to the amplitude of the mean vector wind over the footprint, as modelled by the GMF. Low scatterometer wind speeds are thus providing useful information [22], [23].

The wind variability varies on the globe. This implies for scatterometer measurements, being averaged over a large area, that the Probability Density Function (PDF) of contributing wind directions to a backscatter measurement varies over the globe as well. Wind direction variability acts to reduce the wind direction modulation of the GMF. For example, if wind blows from all directions in a WVC, then wind direction cannot be determined at all. On the other hand, steady winds tend to have higher wind direction GMF modulation than more nominal wind regimes. So, the anisotropy (azimuth direction dependence) of ocean radar backscatter is a function of local wind variability in the WVC (Figure 7).
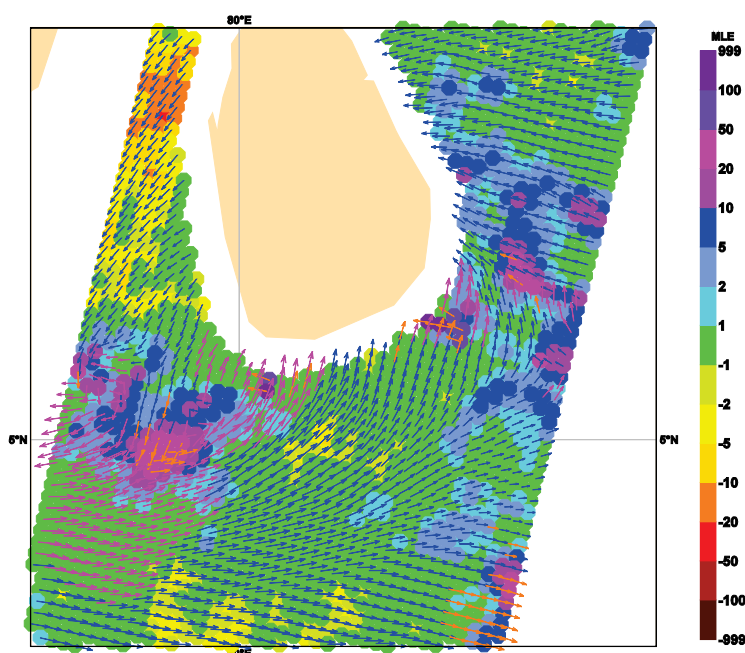

Figure 7: ASCAT wind (arrows) and wind variability (colours) at the ocean surface near Sri Lanka on 25 Nov 2011 3:45 UTC. The maximum winds just south of the island are 20 m/s; some of these wind arrows are coloured purple after flagging by 2DVAR, and some orange, after inversion Quality Control. The wind direction variability (which may be linked to the inversion residual or MLE, see text) is low to the northwest of the island (red colours; steady flow) and very high to the southwest and southeast (purple colours) due to severe convection that caused fatalities on this day.

At high wind speeds wave breaking will further intensify, causing air bubbles, foam and spray at the ocean surface, and a more and more complicated ocean topography. Although theoretically not obvious, it is empirically found that σ^0 keeps increasing for increasing wind speed from 25 m/s to 40 m/s, and that a useful wind direction dependency remains [24], albeit gradually weakening. HH co-polarization (now used for Ku-band scatterometers only) has slightly enhanced sensitivity, but HV and VH polarization (planned for the successor of ASCAT, SCA on EPS-SG) measurements are much more sensitive to extremely high winds than the nominal VV and HH polarizations [24].

3.2. Input screening

Backscatter input products contain flags to denote anomalous (instrument) conditions, which are obviously checked before wind retrieval and no retrieval is done in WVCs where these flags are raised. Examples of such flags are

- The ERS Missing Packet Counters (MPC) and ERS ESA Quality Control flag [25]. If the MPC value is below -18 or above 18, the beam information is rejected. The QC flags for beam arcing and frame checksum error are also evaluated.

- The ASCAT and SCA Sigma0 Usability Flag (must be at least 'usable')

- The OSCAT flags for 'Sigma0 is poor', 'Kp is poor', 'Invalid footprint' and 'Footprint contains saturated slice'.

- For SeaWinds and RapidScat: all bits in the SeaWinds Sigma0 Quality Flag, except the 'Negative' flag.

- For HSCAT unusable backscatter values are coded with value -99 dB or -299 dB in the input data, such values are not used in the wind products.

- For CFOSAT the input data for which the 'Frame usability flag', the 'Sigma0 Measurement Usable Flag' or the 'Low SNR Flag' is set are not used.

Additional tests concern the ranges of the input data, i.e., at least for backscatter values; noise estimates (K_p), azimuth and incidence angles, but also land occurrence and latitude and longitude position. Any data where the values are out of range are not used in the wind processing.

3.3. Atmospheric attenuation

For Ku-band systems, the atmospheric attenuation by water vapour is non-negligible. The attenuation is based on a climatology of water vapour and read from a look-up table, organised on location and the month of the year [26]. The attenuation includes atmospheric oxygen, water vapor, and nominal cloud. A mean global cloud cover of 0.1 mm is assumed. The attenuations contained in the Ku-band wind products for each view are 2-way nadir attenuations in dB at 14 GHz. Prior to wind inversion, the attenuations are divided by the cosine of the view incidence angle to correct for the slant atmospheric path, and subsequently added to σ^0 values.

3.4. Ocean Calibration

Two methods of ocean calibration exist, where NWP Ocean Calibration (NOC) is used operationally. Mean ocean backscatter is quite variable following transient large-scale weather patterns. However, these weather patterns are well analysed in NWP and NWP information may be used to correct for these large-scale variations. Stoffelen [45] introduced NWP Ocean Calibration (NOC) and this method evolved to a powerful procedure to detect instrument anomalies and provide intercalibration of scatterometer systems, i.e., ERS and ASCAT or QuikSCAT and OSCAT. WVC and beam dependent NOC is being employed for ERS [46] and ASCAT [47] in order to provide winds of constant quality. For Ku-band instruments it is also considered [48], but not yet fully implemented, since some issues remain that are not fully understood. Instead, for Ku-band pencil beam instruments a simple but effective NOC calibration method is used. Since no significant signs of azimuth (or WVC) dependent instrument biases are found and the beam incidence angles are constant, we have chosen to apply backscatter

corrections that are only dependent on the beam polarisation. The backscatter corrections (in dB) are chosen such that the wind speed biases between scatterometer winds on the one hand and buoy and NWP winds on the other hand are minimised. The NOC procedure aims to find a representative mean backscatter value for each WVC view, independent of the weather, over a period of a year. NOC may be used for monitoring purposes as well over periods as short as a day or as long as an entire mission [50].

Another and potentially more accurate method is called Cone Metrics (CM), well developed for ASCAT and ERS [49]. This calibration method is independent of NWP input, but provides very similar calibration numbers and wind retrieval residuals. CM is being further developed for Ku-band systems.

3.5. Spatial representation

It is effective for radars to obtain individual backscatter measurements with a rather poor signal-to-noise ratio (SNR) of close to one or higher. In order to get an acceptable SNR on WVC level, multiple data acquisitions are spatially averaged over the WVC area. This results in a WVC level SNR of a few percent which is sufficient to obtain good quality winds. The number of different views (a view being a fixed combination of polarisation, incidence angle, and antenna azimuth angle) contributing to a WVC is generally higher for rotating fan beam instruments like CFOSAT than for fixed fan beam instruments and rotating pencil beam instruments. However, individual measurements are noisier for rotating fan beam instruments, leading to comparable WVC SNR values for all instrument types after averaging.

Each measurement field of view (FOV) has typical dimensions of 10 to 20 km, often smaller in one dimension than in the other, and the FOVs centred in a particular WVC will extend out of the WVC on all sides, leading to some WVC overlap [29]. It also leads to complications in scatterometer wind processing near land and sea ice boundaries and to the development of dedicated products, optimised in coastal regions [51].

The larger the WVC size chosen, the lower the noise in the averaged backscatter values, as more FOVs are integrated. Low noise and larger WVC sizes have advantages in NWP data assimilation, since NWP models do generally not resolve scales below 5-10 times their grid distance, see e.g. [52], [53]. Lower resolution products are obtained by averaging available higher resolution backscatter products. On the other hand, in cases of extreme gradients (large signal), e.g., near polar lows or tropical hurricanes, shift meteorologists may appreciate high resolution winds, at the expense of some additional noise. The choice of spatial averaging approach allows addressing these preferences, after careful validation always ensuring that the resulting spatial representativeness of the data is adequate for the application intended.

In products optimised for coastal regions, for example, only FOVs over water are used to construct WVC backscatter values. This improves the wind coverage in coastal areas, but the WVC positions may be displaced away from the coast due to the exclusion of FOVs over land in the averaging. This leads to slight irregularities in the WVC spacing.

Note that the probability of occurrence of extremely high winds is substantially reduced by spatial averaging, since extreme winds are generally limited in spatial extent. Therefore, scatterometer winds and NWP winds, lacking variability on the smallest scales, are expected to be associated with a narrower wind speed PDF than local buoy winds averaged over 1 or 10 minutes [54], [55].

3.6. NWP collocation

NWP forecast wind data are necessary in the OSI SAF wind processing: for the Ocean Calibration (see section 3.4), for the Ambiguity Removal (3.11), and for product monitoring (3.12). The wind forecasts are used from the ECMWF global model (operational or re-analysis) and they are available twice a day (00 and 12 UTC analysis time, or 06 and 18 UTC analysis in case of the ERA5 re-analysis) with hourly forecast time steps of +3h, +4h, +5h and so on. The model wind data are quadratically interpolated with respect to time and bi-linearly interpolated with respect to location and put into the level 2 information part of each WVC. The ECMWF winds stored in the wind products are stress-equivalent winds [40], which have been computed from the equivalent neutral model winds.

It is important to note that scatterometer winds are being assimilated into the ECMWF model and therefore the wind field used for ambiguity removal (i.e., a forecast) is taken to be independent from the scatterometer observation. In near-real time processing the scatterometer measurement is received at approximately the same time at KNMI and ECMWF, and the scatterometer winds are produced at KNMI within a few minutes typically. Hence the observation cannot yet have been assimilated into the ECMWF model fields at the moment of processing at KNMI.

For scatterometer wind reprocessing, ERA-Interim [56] or ERA5 [57] data are used; here observations are assimilated in the model up to 3 hours after the analysis time. Therefore, in the processing of those observations, only forecast winds starting from 3 hours after analysis time are used. In this way the independence between the scatterometer and the ECMWF model winds, used to guide the wind direction ambiguity removal, is guaranteed.

3.7. Geophysical Model Function

The radar backscatter of the ocean, as derived from the GMF, depends - besides on the wind vector w.r.t. the radar beam pointing - on radar wavelength (C-band or Ku-band) and vertical (VV), horizontal (HH), or cross (HV or VH) polarization. Furthermore, the GMF is a function of incidence angle, wind direction relative to the antenna azimuth angle, and wind speed. As long as the instrument calibrations are correct, the same GMF (for a specific radar band and polarisation) can be used for all instruments. The instrument calibration is checked and if needed backscatter values are corrected using the calibration methods described in section 3.4.

For the OSI SAF C-band scatterometer wind products (ERS and ASCAT), the CMOD7 GMF for calculating stress-equivalent neutral winds is used [34]. CMOD7 is based on CMOD5.n [35]. It is has been developed for intercalibrated ERS and ASCAT C-band scatterometer wind retrievals. As compared to CMOD5.n, CMOD7 better fits the sigma0 triplets at low wind speeds, and it provides more uniform wind speed probability functions across the satellite swath.

Cross-polarization GMFs have been developed from SAR data [36] and will be further improved for SCA. Such GMFs describe the relationship between backscatter and wind speed, with little or no direction information. Day-1 SCA products will utilise the cross-polarised input data for a wind retrieval comparable to what is done for SAR, i.e., using the HV and VH backscatter to compute the wind speed (no direction information) for high speed winds, typically above 20 m/s. For Day-2 SCA products, the cross-polarised information will be used in the wind retrieval using the three VV beams and VH beam together to get the best wind estimate from all combined backscatter information.

For the OSI SAF Ku-band scatterometer wind products (like SeaWinds, OSCAT and RapidScat) the NSCAT-2 GMF for calculating U10S was used in the past [31]. Portabella ([11]; appendix C) compared the QSCAT-1 [33] and NSCAT-2 Ku-band GMFs for SeaWinds wind retrieval. He found that the QSCAT-1 results in more wind solutions during wind retrieval, i.e., it is more ambiguous. In other words, for QSCAT-1 we generally find more minima when we inspect the *MLE* as a function of wind direction. Portabella verified that the additional minima are generally artificial and do not contribute to wind direction skill, i.e., act as a noise source. These additional local minima (noise) in the inversion potentially do result in local minima in ambiguity removal, even when using the so-called Multiple Solution Scheme (MSS), and thus in locally erroneous scatterometer wind field retrieval (see section 3.11).

A known problem of NSCAT-2 is that it overestimates wind speeds above 15 m/s, both when comparing to buoy winds and to NWP model winds. Hence, the NSCAT-2 GMF was changed for wind speeds above 15 m/s. The new GMF is called NSCAT-4. The NSCAT-4 GMF was derived from the NSCAT-2 GMF. Above 15 m/s, a linear scaling of the wind speed was applied. Subsequently, 0.2 m/s was added to all wind speeds to represent U10S.

$v_{NSCAT-4} = v_{NSCAT-2} + 0.2;$ $\qquad$ $v <= 15$ m/s

$v_{NSCAT-4} = 2/3 * v_{NSCAT-2} + 5.2;$ $\qquad$ $v > 15$ m/s

So, a backscatter value leading to an 8 m/s wind from NSCAT-2 corresponds to a 8.2 m/s NSCAT-4 wind and a 24 m/s wind from NSCAT-2 corresponds to a 21.2 m/s NSCAT-4 wind retrieval. The NSCAT-2 GMF lookup table was adapted in this way for all combinations of incidence and azimuth angles. This ensures that the fit in measurement space of the backscatter quadruplets to the GMF will not change. In [32] it was shown that NSCAT-4 provides a good fit of scatterometer wind speeds to both ECMWF and buoy winds. Recently, NSCAT-4 has been improved further using direct ScatSat-1 and ASCAT collocations, in order to bring the Ku-band wind direction distributions closer to those from ASCAT and to match the wind speed probability distribution functions. This has resulted in the NSCAT-4DS GMF (NSCAT-4 with direction and speed corrections) [66]. The newer near-real time Ku-band wind products from HY-2B, HY-2C, HY-2D, and CFOSAT and the new Ku-band climate data records use NSCAT-4DS.

An aspect which is particularly relevant for Ku-band wind retrievals is the Sea Surface Temperature (SST) dependence of the radar backscatter. Comparison of collocated winds from ASCAT (C-band) on one hand and RapidScat or ScatSat-1 on the other hand has shown that the Ku-band backscatter varies due to SST changes, depending on scatterometer radar frequency, polarization, and incidence angle. For C-band however, such variations are negligible [67]. Inverse backscatter modifications have been computed to compensate for the GMF SST dependencies [68]; these modifications are used in the newer near-real time Ku-band wind products from HY-2B, HY-2C, HY-2D, and CFOSAT and in the new Ku-band climate data records.

3.8. Wind retrieval

In scatterometer wind retrieval a Geophysical Model Function (GMF) is inverted. The inversion step combines the backscatter measurements in a WVC to compute the WVC-mean wind vector. Due to

their different geometries, subtle, but very relevant, differences exist in the inversion steps of C-band fan-beam and Ku-band scatterometers, with either rotating fan or pencil beams. For rotating fan beam instruments, the number of inputs (views) to the wind retrieval is generally higher than for other instruments, but it doesn't change the principle of the wind retrieval since each view is associated with a unique query on the Geophysical Model Function (GMF).

3.8.1. C-band scatterometers

The GMF has two unknowns, namely wind speed and wind direction. So, if more than two backscatter measurements with Gaussian noise are available then these two unknowns may be estimated using a quadratic estimator as the objective function for determining the wind vector [27]. Based on Bayes' probability theorem, the Maximum Likelihood Estimator, *MLE,* is redefined by ([20], Chapter II):

$$MLE = \frac{1}{SD^2} \sum_{i=1}^{N} \left(z_{o,i} - z_{m,i} \right)^2$$

where $z_{o,i}$ are the backscatter measurements, $z_{m,i}$ are the simulated backscatter values corresponding to the measurements, $i \in (1,N)$, and *SD* is a measure of the measurement set noise standard deviation, related to both instrument noise and geophysical noise [28], [29]; $z = (\sigma^0)^{0.625}$ is a transformation that limits the wind direction sensitivity of the GMF to two harmonics. The wind direction sensitivity of the *MLE* function above is then approximately constant for the ERS and ASCAT fan-beam scatterometers and thus makes the inversion problem linear [28] and the *MLE* minima quadratic. The *MLE* value represents the probability of a trial wind vector (solution) being the 'true' wind, where higher *MLE*s correspond to lower probabilities and vice versa. Thus the wind inversion procedure consists of finding the minima in the *MLE*. The inversion of ERS and ASCAT measurement sets usually results in two well-defined local minima of the *MLE,* corresponding to two opposing wind vector solutions. The three independent measurements generally well sample the azimuth variation of the GMF and resolve the wind direction, albeit ambiguously.

3.8.2. Ku-band scatterometers

In [28], Bayes' retrieval for the varying azimuth geometry of pencil-beam scatterometers is discussed and it is noted that such scatterometers are not sensitive to the wind vector for certain wind directions, which systematically vary by WVC. Therefore, the inversion procedure cannot be made linear and broad and skew *MLE* minima remain near these wind directions. Moreover, these wind directions "attract" local *MLE* minima and thus these local minima do not necessarily represent an optimal solution. The inherent broad and skew minima of pencil-beam scatterometers may be well represented in the wind vector solution space by the MSS that is used in the OSI SAF wind products [43]. In fact, for each wind direction the optimal speed is selected by minimizing a MLE in σ^o space and its residual (*MLE*) is kept. The residuals are converted to probabilities, which are used in the ambiguity removal for all wind directions simultaneously, thus representing the full wind vector solution probability density function at each WVC.

3.9. Quality control

Since the scatterometer wind retrieval problem is over-determined, this opens up the possibility of quality control (QC) by checking the inversion residual. The inversion residual (*MLE*) is in theory inversely proportional to the log probability that a WVC is affected solely by a nominal, representative

wind vector. Generally such probability is low, and the wind vector solution residual high, when there is substantial wind or sea state variability within the cell or when rain affects the WVC for Ku-band scatterometers [28], [29], [30].

As such, Portabella and Stoffelen [41] found that the inversion residual is well capable of removing cases with extreme wind variability (at fronts or centres of lows), or with other geophysical variables affecting the radar backscatter, such as rain. QC is performed on the WVCs and rejection percentages vary between 3-7% for Ku-band and are well below 1% for C-band systems. The KNMI QC procedure proves very effective, among others for screening rain in Ku-band scatterometers [60].

Steady flows show an increased harmonic dependence (anisotropy) of ocean radar backscatter and thus an elevated absolute *MLE* due to relatively poor correspondence with the GMF which has been derived for nominal wind conditions. Portabella et al. [61] found that the derived wind vectors are of good quality in such cases, but are degraded in cases of relatively isotropic ocean response. The latter are caused by (extreme) wind variability, rain splash [64] or perhaps confused sea states, which hamper the derivation of a representative wind vector. Therefore, a QC procedure has been implemented (for ERS and ASCAT) that only flags cases of increased isotropic response of the ocean backscatter [61].

The QC skill for Ku-band wind retrievals has been improved recently with the use of the so-called J_{oss} parameter which is computed from the analysis wind field in the 2DVAR ambiguity removal step. This results in a lower rejection rate of potentially suspect winds [63]. Two new QC flags for Ku-band wind scatterometry are implemented, a conservative (NWP QC) flag to replace the old KNMI *MLE* flag for NWP applications, and a new, less conservative (nowcasting QC) flag for nowcasting applications. The NWP QC flag shows a better QC skill than the old *MLE* flag but at the same time it rejects significantly less winds. The nowcasting QC flag shows a comparable skill as the old *MLE* flag and it rejects even less winds. For C-band scatterometry (having much lower QC rejection rates) the QC is still only based on the *MLE*.

3.10. Sea ice screening

Following the developments on Bayesian wind retrieval, [16] and [17] provide scatterometer sea ice GMF and retrieval procedures. In fact, combining both wind and sea ice retrievals, the probability of sea ice may be computed, which shows very good sensitivity of scatterometer systems to sea ice cover, including over the melt season where passive microwave techniques appear less sensitive [16]. NWP model sea surface temperature (SST) data are used to support the Bayesian sea ice discrimination. WVCs with a sea surface temperature above 5 °C are assumed to be always open water. The ice screening procedure may sometimes assign rainy WVCs erroneous as ice; using the extra SST criterion, WVCs in warmer areas will never be labelled as ice. Due to its rather high threshold value, the NWP SST ice screening will only be active in regions far away from the poles. The Bayesian sea ice screening is used both for C-band and Ku-band instrument data, except for ISS/RapidScat which does hardly observe any sea ice areas due to its lower orbit inclination. For RapidScat a simple discrimination based on ECMWF SST data is used. For CFOSAT, the Bayesian ice screening algorithm can also be used in principle, but it is technically more complicated due to the larger number of views present in each WVC [65]. An algorithm will be developed, until then a simple discrimination based on ECMWF SST data is used as well.

3.11. Ambiguity Removal

Scatterometer winds have multiple ambiguities and there are up to four local minima after wind inversion in each WVC. These may be well-defined inversion minima, but also broad and skew minima (see section 3.8.2). The ambiguities are removed by applying constraints on the spatial characteristics of the output wind field, such as on rotation and divergence. The 2DVAR scheme closely resembles the 3D-var and 4D-var schemes applied in NWP data assimilation. Several ambiguity removal (AR) schemes were evaluated for ERS data [42]. In addition to the subjective comparison of AR schemes, a method for the objective comparison of AR performance among the different schemes was used. In [42] it is shown that this way of comparison is effective to evaluate the shortcomings of AR schemes, but also reveals a more general way forward to improve AR, which is followed up by adapting 2DVAR [58].

2DVAR uses a short-range NWP wind forecast valid at the time and location of the scatterometer measurements and subtracts it from the scatterometer wind solutions. The resulting ambiguous innovations and their probabilities are represented in the ambiguous scatterometer observation operator ([20], Chapter V). Vogelzang et al. [59] evaluate the general spatial covariance structure of these innovations and successfully apply the found NWP error covariance matrices in 2DVAR. Scatterometer observation errors appear generally spatially uncorrelated. The rotation and divergence structures in the specified NWP error covariances in 2DVAR have a clear effect on 2DVAR performance, while the quality of the prior forecast information appears less critical [58], [42].

To represent the variable inversion minima in the rotating-beam scatterometer processing, MSS is used. The probability density function of the wind solutions is represented by binning the full circle of possible wind directions into 144 equal sectors of 2.5° and for each wind direction an optimal wind speed with its corresponding probability is calculated in the wind retrieval step. Subsequently, the 144 solutions of each WVC are used in the AR to select the optimal solution.

3.12. Product monitoring

For global coverage products, it is possible to generate a product monitoring flag, based on a multi-step check. If in one product the number of WVC Quality Control rejections, the mean residual (*MLE*), or the wind speed bias with respect to the ECMWF NWP background is above certain threshold values, typically 5 times the RMS in the expected nominal values, then the monitoring event flag is raised since the product is suspicious. The threshold values are based on evaluation of the product statistics over a long period and maximise the probability of detection while minimising the false alarm rate [44].

In the case when the scatterometer product is not global but granular (like the ASCAT regional EARS products) and files containing only a few minutes of data are generated and disseminated in real-time, this mechanism raises problems if there are not enough data in one pass for a statistically valid check. The multi-step monitoring check is sensitive to noise which is larger when mean values are calculated over fewer WVCs. If, accordingly, the thresholds are set high, many bad products will pass the check. On the other hand, if the threshold values are set too low, too many false alarms will be raised. This problem is solved by evaluating not only the data of the last processed pass, but by evaluating an amount of most recent data equivalent to the amount of half an orbit, although possibly originating from several different read-outs. In case of instrument degradation or other problems, the monitoring event flag will be raised with some delay, inherent to the discontinuous nature of a regional data stream.

4. Wind processing

KNMI has wind processing chains in place for several instruments, currently for Metop/ASCAT, HY-2B/HSCAT, HY-2C/HSCAT, HY-2D/HSCAT, and CFOSAT/RFSCAT in near-real time. The near-real time processing of the scatterometer backscatter data to a wind product is done on KNMI's operational computing facilities. Reprocessing facilities exist or will be created for ERS/SCAT, Metop/ASCAT, QuikSCAT/SeaWinds, ISS/RapidScat, and Oceansat-2/OSCAT.

The wind processing software is developed within the OSI SAF and consists of a generic part (called genscat) and a part that is specially designed to handle the data of a specific instrument. The genscat software consists of several modules devoted to e.g. reading and writing of BUFR and NetCDF data, collocation of scatterometer data with NWP fields, wind inversion and ambiguity removal. The instrument specific part of the software contains the main program control; it calls the different modules and routines in order to execute the processing steps as outlined in Figure 5.

Ancillary data from the ECMWF global model are present on a central location of the computing facilities. Scatterometer input swath data are normally received through the EUMETCast system. The granularity of the input data is different per product type: one input file containing from 3 minutes of data for ASCAT global products up to one orbit (~100 minutes of data) for other satellites. The granularity of the BUFR output data is the same as the granularity of the input data, for level 2 NetCDF the output data are always organised per orbit. Please see the corresponding Product User Manuals for more detailed information.

In the near-real time processing chains, a run control script is executed every few minutes and checks if any new data has arrived. If so, the new files are copied from the EUMETCast reception station location to a local directory, the NWP data valid at the time of the measurements is searched and the scatterometer data files are processed one by one. Each input file usually results in one output file containing wind data. Output files are sent to the KNMI FTP server, to the EUMETCast uplink station and to the GTS where appropriate.

In the reprocessing chains, long time series of wind products are created. Scatterometer and ECMWF input data are collected first from different archives and then the data processing and monitoring of the whole data set is controlled by a script. The reprocessing is not different from near-real time processing in terms of algorithm, it is different only in the way that archive data are used and that the latest version of the wind processing software is used, see the respective Product User Manuals for more information of the used software. Moreover, reanalysis ECMWF data are used (ERA-Interim in the OSI SAF CDOP2 phase or ERA5 in the CDOP3 phase) in the reprocessing chains rather than data from the operational ECMWF model.

5. References

[1] A. Stoffelen et al., Scientific Developments and the EPS-SG Scatterometer, *IEEE Journal of Selected Topics in Applied Earth Observations and Remote Sensing*, 2017, vol. 10, no. 5, pp. 2086-2097, doi:10.1109/JSTARS.2017.2696424

[2] Isaksen, L., and A. Stoffelen, ERS-Scatterometer Wind Data Impact on ECMWF's Tropical Cyclone Forecasts, *IEEE-Transactions on Geoscience and Remote Sensing*, 2000, <u>38</u> (4), 1885-1892

[3] Stoffelen, A., R. Kumar, J. Zou, V. Karaev, P. Chang, and E. Rodriguez, Ocean Surface Vector Wind Observations, *Remote Sensing of the Asian Seas*, 429-447, Eds.: Vittorio Barale, Martin Gade, Springer, 2018, ISBN 3319940678, 9783319940670, 565 pages

[4] Bourassa, M., T. Meissner, I. Cerovecki, P. Chang, X. Dong, G. De Chiara, C. Donlon, D. Dukhovskoy, J. Elya, A. Fore, M. Fewings, R. Foster, S. Gille, B. Haus, S. Hristova-Veleva, H. Holbach, Z. Jelenak, J. Knaff, S. Kranz, A. Manaster, M. Mazloff, C. Mears, A. Mouche, M. Portabella, N. Reul, L. Ricciardulli, E. Rodriguez, C. Sampson, D. Solis, A. Stoffelen, M. Stukel, B. Stiles, D. Weissman, F. Wentz, Remotely Sensed Winds and Wind Stresses for Marine Forecasting and Ocean Modeling, *Frontiers in Marine Science*, 2019, 6, p. 443+, doi:10.3389/fmars.2019.00443, https://www.frontiersin.org/article/10.3389/fmars.2019.00443, ISSN=2296-7745.

[5] Belmonte Rivas, M., Stoffelen, A., Characterizing ERA-Interim and ERA5 surface wind biases using ASCAT, *Ocean Sci*. 2019, 15 (3), 831-852, DOI: 10.5194/os-15-831-2019.

[6] Vogelzang, J., A. Verhoef, J. Verspeek, J. de Kloe and A. Stoffelen, AWDP User Manual and Reference Guide, version 3.0, NWPSAF-KN-UD-005, 2016.

[7] Verhoef, A., J. Vogelzang, J. Verspeek and A. Stoffelen, PenWP User Manual and Reference Guide version 2.0, NWPSAF-KN-UD-009, 2015

[8] Li, Z., A. Verhoef and A. Stoffelen, CWDP User Manual and Reference Guide, SAF/OSI/KNMI/TEC/MA/320

[9] Belmonte Rivas, M., Otosaka, I., Stoffelen, A., and Verhoef, A.: A scatterometer record of sea ice extents and backscatter: 1992–2016, *The Cryosphere*, 2018, 12, 2941-2953, doi:10.5194/tc-12-2941-2018

[10] L. Brocca, C. Massari, L. Ciabatta, W. Wagner and A. Stoffelen, Remote Sensing of Terrestrial Rainfall From Ku-Band Scatterometers, *IEEE Journal of Selected Topics in Applied Earth Observations and Remote Sensing*, 2016, vol. 9, no. 1, pp. 533-539, doi:10.1109/JSTARS.2015.2508065.

[11] Portabella, M, thesis "Wind Field Retrieval from Satellite radar systems", 2002 (*)

[12] See https://earth.esa.int/web/sppa/mission-performance/esa-missions/ers-1/scatterometer/sensor-description and https://earth.esa.int/web/sppa/mission-performance/esa-missions/ers-2/scatterometer/sensor-description

[13] Portabella, M. and A. Stoffelen, A comparison of KNMI Quality Control and JPL Rain Flag for SeaWinds, *Canadian Journal of Remote Sensing*, 2002, 28, 3, 424-430, doi:10.5589/m02-040.

[14] J. Vogelzang; A. Stoffelen, ASCAT Ultrahigh-Resolution Wind Products on Optimized Grids, *IEEE Journal of Selected Topics in Applied Earth Observations and Remote Sensing*, 2017, vol.10, no.5, pp. 2332-2339, doi:10.1109/JSTARS.2016.2623861

[15] D. G. Long, Polar Applications of Spaceborne Scatterometers, *IEEE Journal of Selected Topics in Applied Earth Observations and Remote Sensing*, 2017, vol. 10, no. 5, pp. 2307-2320, doi:10.1109/JSTARS.2016.262941

[16] Belmonte Rivas, M. and A. Stoffelen, New Bayesian algorithm for sea ice detection with QuikSCAT, *IEEE Transactions on Geoscience and Remote Sensing*, 2011, <u>49</u>, 6, 1894-1901, doi:10.1109/TGRS.2010.2101608.

[17] Belmonte, M., J. Verspeek, A. Verhoef and A. Stoffelen, Bayesian sea ice detection with the Advanced Scatterometer, *IEEE Transactions on Geoscience and Remote Sensing*, 2012, <u>50</u>, 7, 2649-2657, doi:10.1109/TGRS.2011.2182356.

[18] Valenzuela, G. R., Theories for the interaction of electromagnetic and ocean waves - a review, *Bound. Layer Meteor.*, 1978, 13, 612-685

[19] Fois, F., Enhanced Ocean Scatterometry, Thesis: Technische Universiteit Delft, 2015, Delft, http://repository.tudelft.nl/islandora/object/uuid:06d7f7ad-36a9-49fa-b7ae-ab9dfc072f9c/datastream/OBJ/download.

[20] Stoffelen, A., thesis "Scatterometry", 1998, http://dspace.library.uu.nl/bitstream/handle/1874/636/full.pdf

[21] Donelan, M. A., and W. J. Pierson, Radar scattering and equilibrium ranges in wind-generated waves with application to scatterometry, *J. Geophys. Res.*, 1987, <u>92</u>, 4971-5029

[22] Plant, W. J., Effects of wind variability on scatterometry at low wind speeds, *J. Geophys. Res.*, 2000, <u>105</u> (C7), 16,899–16,910, doi:10.1029/2000JC900043

[23] Shankaranarayanan, K., and M. A. Donelan, A probabilistic approach to scatterometer model function verification, *J. Geophys. Res.*, 2001, <u>106</u> (C9), 19,969–19,990, doi:10.1029/1999JC000189

[24] Fernandez, D. E., J. R. Carswell, S. Frasier, P. S. Chang, P. G. Black, and F. D. Marks, Dual-polarized C- and Ku-band ocean backscatter response to hurricane-force winds, *J. Geophys. Res.*, 2006, <u>111</u>, C08013, doi:10.1029/2005JC003048

[25] Met Office, UK, ERS Products, WMO FM94 BUFR format, ER-IS-UKM-GS-0001, Version 4, Issue 2, 16 February 2001

[26] Wentz, F.J., Final Delivery: Climatology of 14-GHz Atmospheric Attenuation, report number 052096, Remote Sensing Systems, 1996

[27] Pierson, W.J., Probabilities and statistics for backscatter estimates obtained by a scatterometer, *J. Geophys. Res.*, 1989, <u>94</u>, 9743-9759; correction in *J. Geophys. Res.*, 1990, <u>95</u>, 809

[28] Stoffelen, A. and M. Portabella, On Bayesian Scatterometer Wind Inversion, *IEEE Transactions on Geoscience and Remote Sensing*, 2006, <u>44</u>, 6, 1523-1533, doi:10.1109/TGRS.2005.862502.

[29] Portabella, M. and A. Stoffelen, Scatterometer backscatter uncertainty due to wind variability, *IEEE Transactions on Geoscience and Remote Sensing*, 2006, <u>44</u>, 11, 3356-3362, doi:10.1109/TGRS.2006.877952.

[30] W. Lin, M. Portabella, A. Stoffelen, A. Verhoef and A. Turiel, ASCAT Wind Quality Control Near Rain, *IEEE Transactions on Geoscience and Remote Sensing*, 2015, vol. 53, no. 8, pp. 4165-4177, doi:10.1109/TGRS.2015.2392372

[31] Wentz, F.J., D.K. Smith, A model function for the ocean normalized radar cross section at 14 GHz derived from NSCAT observations, *J. Geophys. Res.*, 1999, 104 (C5), 11499-11514, doi:10.1029/98JC02148

[32] Verhoef, A., and A. Stoffelen, OSCAT winds validation report, OSI SAF report, SAF/OSI/CDOP2/KNMI/TEC/RP/196, 2012 (*)

[33] Jet Propulsion Laboratory, QuikSCAT Science Data Product User's Manual, version 3.0, JPL D-18053, 2006

[34] Stoffelen, A., J. Verspeek, J. Vogelzang and A. Verhoef, The CMOD7 Geophysical Model Function for ASCAT and ERS Wind Retrievals, *IEEE Journal of Selected Topics in Applied Earth O*, 2017, 10, 5, 2123-2134, doi:10.1109/JSTARS.2017.2681806

[35] Verhoef, A., M. Portabella, A. Stoffelen and H. Hersbach, CMOD5.n - the CMOD5 GMF for neutral winds, OSI SAF report, SAF/OSI/CDOP/KNMI/TEC/TN/165, 2008 (*)

[36] Mouche, A., B. Chapron, J. Knaff, Y. Zhao, B. Zhang, C. Combot, Copolarized and Cross-Polarized SAR Measurements for High-Resolution Description of Major Hurricane Wind Structures: Application to Irma Category 5 Hurricane, *JGR Oceans*, 2019, 124, 6, 3905-3922, doi: 10.1029/2019JC015056

[37] Portabella, M. and A. Stoffelen, On Scatterometer Ocean Stress, *J. Atm. Oceanic Technol.*, 2009, 26, 2, 368-382 (*)

[38] Hersbach, H., Assimilation of scatterometer data as equivalent-neutral wind, *ECMWF Technical Memorandum* 629, 2010

[39] ECMWF, Official IFS Documentation, Available through https://www.ecmwf.int/

[40] De Kloe, J., A. Stoffelen and A. Verhoef, Improved Use of Scatterometer Measurements by using Stress-Equivalent Reference Winds, *IEEE Journal of Selected Topics in Applied Earth O,* 2017, 10, 5, 2340-2347, doi:10.1109/JSTARS.2017.2685242

[41] Portabella, M., Stoffelen, A., Quality Control and Wind Retrieval for SeaWinds, EUMETSAT fellowship report, 2002 (*)

[42] Stoffelen, A., S. de Haan, Y. Quilfen, and H. Schyberg, ERS Scatterometer Ambiguity Removal Comparison, OSI SAF report, 2000 (*)

[43] Portabella, M. and A. Stoffelen, A probabilistic approach for SeaWinds data assimilation, *Quart. J. Royal Meteor. Soc.*, 2004, 130, 127-152

[44] de Vries, J., A. Stoffelen J. and Beysens, Ambiguity Removal and Product Monitoring for SeaWinds, NWP SAF report NWPSAF_KN_TR_001 (*)

[45] Stoffelen, A., A Simple Method for Calibration of a Scatterometer over the Ocean, *J. Atmos. Ocean. Technol.*, 1999, 16 (2), 275-282 (See [20], Appendix A (*))

[46] Stoffelen, A., J. Vogelzang and A. Verhoef, Verification of scatterometer winds, 10th International Winds Workshop, 20/2/2010-26/2/2010, M. Forsythe & J. Daniels (Ed), 2010, Tokyo, Japan, JMA, EUMETSAT (*)

[47] Verspeek, J., A. Stoffelen, A. Verhoef and M. Portabella, Improved ASCAT Wind Retrieval Using NWP Ocean Calibration, *IEEE Transactions on Geoscience and Remote Sensing*, 2012, 50, 7, 2488-2494, doi:10.1109/TGRS.2011.2180730 (*)

[48] Risheng, Y., A. Stoffelen, J. Verspeek and A. Verhoef, NWP Ocean Calibration of Ku-band scatterometers, IGARSS 2012 (IEEE), 22/7/2012-27/7/2012, 2012, Munich, Germany (*)

[49] M. B. Rivas, A. Stoffelen, J. Verspeek, A. Verhoef, X. Neyt and C. Anderson, Cone Metrics: A New Tool for the Intercomparison of Scatterometer Records, *IEEE Journal of Selected Topics in Applied Earth Observations and Remote Sensing*, vol. 10, no. 5, pp. 2195-2204, 2017, doi:10.1109/JSTARS.2017.2647842

[50] Anderson, C., J. Figa, H. Bonekamp, J. Wilson, J. Verspeek, A. Stoffelen and M. Portabella, Validation of Backscatter Measurements from the Advanced Scatterometer on MetOp-A, *J. Atm. Oceanic Technol.*, 2012, 29, 77-88, doi:10.1175/JTECH-D-11-00020.1 (*)

[51] Verhoef, A., M. Portabella and A. Stoffelen, High-resolution ASCAT scatterometer winds near the coast, *IEEE Transactions on Geoscience and Remote Sensing*, 2012, 50, 7, 2481-2487, doi:10.1109/TGRS.2011.2175001 (*)

[52] Skamarock, W. C., Evaluating Mesoscale NWP Models Using Kinetic Energy Spectra, *Monthly Weather Review* 132, Dec. 2004, 3019-3032

[53] Ad Stoffelen, Jur Vogelzang en Gert-Jan Marseille, High resolution data assimilation guide, v1.2 (NWPSAF-KN-UD-008) (*).

[54] Vogelzang, J., A. Stoffelen, A. Verhoef and J. Figa-Saldaña, On the quality of high-resolution scatterometer winds, *J. of Geophysical Research*, 2011, 116, C10033, doi:10.1029/2010JC006640 (*)

[55] Stoffelen, A., A. Mouche, M. Portabella, W. Lin, F. Polverari, G. J. van Zadelhoff, P. Chang, Z. Jenenak, J. Sapp, J. Bidlot, and M. Bourassa, C-band High and Extreme Force Speeds (CHEFS) https://mdc.coaps.fsu.edu/scatterometry/meeting/docs/2018/docs/WednesdayApril25/WednesdayMorning/CHEFS.pptx .

[56] Dee, D.P. et al., The ERA-Interim reanalysis: configuration and performance of the data assimilation system, *Q.J.R. Meteorol. Soc.,* 2011, 137, 553-597. doi:10.1002/qj.828

[57] Hersbach, H, B. Bell, P. Berrisford et al., The ERA5 global reanalysis, *Q J R Meteorol Soc.,* 2020, 146, 1999-2049, doi:10.1002/qj.3803

[58] Vogelzang, J., A. Stoffelen, A. Verhoef, J. de Vries and H. Bonekamp, Validation of two-dimensional variational ambiguity removal on SeaWinds scatterometer data, *J. Atm. Oceanic Technol.*, 2009, 7, 26, 1229-1245, doi:10.1175/2008JTECHA1232.1 (*).

[59] Vogelzang, J, and A. Stoffelen, Improvements in Ku-band scatterometer wind ambiguity removal using ASCAT-based empirical background error correlations, *Q J R Meteorol Soc.* 2018, 144, 2245-2259, doi:10.1002/qj.3349

[60] Portabella, M. and A. Stoffelen, Rain Detection and Quality Control of SeaWinds, *J. Atm. Oceanic Technol.*, 2001, 18, 7, 1171-1183, doi:10.1175/1520-0426(2001)018<1171:RDAQCO>2.0.CO;2

[61] Portabella, M., A. Stoffelen, A. Verhoef and J. Verspeek, A new method for improving ASCAT wind quality control, *IEEE Geosci. Remote Sensing Letters*, 2012, 9, 4, 579-583, doi:10.1109/LGRS.2011.2175435 (*).

[62] Portabella, M., A. Stoffelen, W. Lin, A. Turiel, A. Verhoef, J. Verspeek and J. Ballabrera-Poy, Rain Effects on ASCAT-Retrieved Winds: Toward an Improved Quality Control, *IEEE Transactions on Geoscience and Remote Sensing*, 2012, 50, 7, 2495-2506, doi:10.1109/TGRS.2012.2185933 (*).

[63] Verhoef, A. and A. Stoffelen, Advances in Ku-band scatterometer Quality Control, OSI SAF report SAF/OSI/CDOP3/KNMI/SCI/TN/404, 2021 (*)

[64] Lin, C.C., M. Betto, M. Belmonte-Rivas, A. Stoffelen and J. de Kloe, EPS-SG Wind Scatterometer Concept Trade-offs and Wind Retrieval Performance Assessment, *IEEE Transactions on Geoscience and Remote Sensing*, 2012, 50, 7, 2458-2472, doi:10.1109/TGRS.2011.2180393 (*).

[65] Li, Z., A. Stoffelen and A. Verhoef, A generalized simulation capability for rotating-beam scatterometers, *Atmos. Meas. Tech.*, 2019, 12, 3573–3594, doi:10.5194/amt-12-3573-2019

[66] Wang, Z., A. Stoffelen, B. Zhang, Y. He, W. Lin, X. Li, Inconsistencies in scatterometer wind products based on ASCAT and OSCAT-2 collocations, *Remote Sensing of Environment*, 2019, 225, 207-216, doi:10.1016/j.rse.2019.03.005

[67] Wang, Z., A. Stoffelen, F. Fois, A. Verhoef, C. Zhao, M. Lin and G. Chen, SST Dependence of Ku- and C-band Backscatter Measurements, IEEE *Journal of Selected Topics in Applied Earth O*, 2017, 10, 5, 2135-2146, doi:10.1109/JSTARS.2016.2600749

[68] Wang, Z., A. Stoffelen, C. Zhao, J. Vogelzang, A. Verhoef, J. Verspeek, M. Lin and G. Chen, An SST-dependent Ku-band geophysical model function for RapidScat, *JGR Oceans*, 2017, 122, 4, 3461-3480, doi:10.1002/2016JC012619

References marked with a (*) are available on https://scatterometer.knmi.nl/publications/.

6. Abbreviations and acronyms

2DVAR	Two-dimensional Variational Ambiguity Removal
AR	Ambiguity Removal
ASCAT	Advanced Scatterometer
AWDP	ASCAT Wind Data Processor
CDOP	Continuous Development and Operations Phases of the SAFs
CFOSAT	China-France Oceanography SATellite
CWDP	CFOSAT Wind Data Processor
EN	Equivalent Neutral
EPS-SG	Second Generation of the European Polar Satellites
ERS	European Remote-Sensing Satellite
EARS	EUMETSAT Advanced Retransmission Service
EUMETCast	EUMETSAT's Digital Video Broadcast Data Distribution System
EUMETSAT	European Organisation for the Exploitation of Meteorological Satellites
GMF	Geophysical Model Function
HH	Horizontal polarisation of sending and receiving radar antennas
HSCAT	Scatterometer on-board the Chinese Haiyang satellites
JPL	Jet Propulsion Laboratory (NASA)
KNMI	Royal Netherlands Meteorological Institute
Kp	Backscatter measurement noise estimate
MLE	Maximum Likelihood Estimator
MSS	Multiple Solution Scheme
NASA	National Aeronautics and Space Administration (USA)
NOAA	National Oceanic and Atmospheric Administration (USA)
NOC	NWP Ocean Calibration
NSCAT	NASA Scatterometer
NWP	Numerical Weather Prediction
OSCAT	Scatterometer on-board the Indian Oceansat-2 and ScatSat-1 satellites
OSI SAF	Ocean and Sea Ice SAF
PenWP	Pencil Beam Wind Processor
PDF	Probability Density Function
QC	Quality Control
QuikSCAT	USA dedicated scatterometer mission

RapidScat	SeaWinds-like scatterometer on-board the International Space Station
SAF	Satellite Application Facility
SCA	Scatterometer on EPS-SG, the successor of ASCAT
SE	Stress Equivalent
SeaWinds	Scatterometer on-board QuikSCAT platform (USA)
SST	Sea Surface Temperature
u	West-to-east wind component
v	South-to-north wind component
VV	Vertical polarisation of sending and receiving radar antennas
WMO	World Meteorological Organization
WVC	Wind Vector Cell